

# Climatic and geological insights on geochemical signatures left in ancient glass

Bongsu Chang<sup>1</sup>, Bum Ki Lee<sup>2</sup>, Jieun Seo<sup>1</sup>, Sun Ki Choi<sup>3</sup>, Seon-Gyu Choi<sup>1</sup>,  
Yeontae Jo<sup>4</sup>, Seon Yong Lee<sup>5</sup>, Young Jae Lee<sup>1\*</sup>

<sup>1</sup>*Department of Earth and Environmental Sciences, Korea University, Seoul 02841, Republic of Korea ([bschang@korea.ac.kr](mailto:bschang@korea.ac.kr); [still4@korea.ac.kr](mailto:still4@korea.ac.kr); [seongyu@korea.ac.kr](mailto:seongyu@korea.ac.kr))*

<sup>2</sup>*Jeonnam Research Institute of Cultural Heritage, Muan 58566, Republic of Korea ([baumki@hanmail.net](mailto:baumki@hanmail.net))*

<sup>3</sup>*Ocean Georesources Research Department, Korea Institute of Ocean Science and Technology, Busan 49111, Republic of Korea ([chlsunki@kiost.ac.kr](mailto:chlsunki@kiost.ac.kr))*

<sup>4</sup>*Conservation Science Division, National Museum of Korea, Seoul 04383, Republic of Korea ([yeontae@korea.kr](mailto:yeontae@korea.kr))*

<sup>5</sup>*Geo-Environmental Research Center, Korea Institute of Geoscience and Mineral Resources, Daejeon 34132, Republic of Korea ([seonyonglee@kigam.re.kr](mailto:seonyonglee@kigam.re.kr))*

\*Corresponding author. E-mail: [youngjlee@korea.ac.kr](mailto:youngjlee@korea.ac.kr)

## Abstract

Glass artifacts have been the subject of extensive trade as exquisite items of the social elite since ancient times. Vestiges of their production and migration are still visible around the globe. To comprehend the historical narrative of human life encapsulated within them, it is imperative to ascertain their inception, which directly correlates with the identification of raw materials used in glassmaking. This is attributed to the material's distinctiveness, enabling it to aptly reflect the climatic and geological characteristics of the respective geographic location where the glass is produced. However, glass, made through the fusion of raw materials, retains only its bulk chemistry, lacking visual and mineralogical associations with the input. Here, we compiled thousands of accessible glass analyses, demonstrating a link between geographic origins and geochemical signatures of the artifacts, and delineated the climatic and geological implications of these signatures. Climatic differences across regions influence geological processes systematically, resulting in environments characterized by unique geochemical signatures. These signatures are reflected in anomalous elemental signals indicative of specific raw materials used in glass production. Additionally, analysis of rare-earth element patterns provides further confirmation of the inferred flux sources and regional origins. We anticipate our assay to serve as a solid foundation for providing a clearer and more visual representation of the ancient East–West glass trade.

**Keywords:** *Ancient glass; Geographical origin; Multivariate analysis; Rare-earth element; Geology; Climate*

# Statements and Declarations

## Competing interests

All authors certify that they have no affiliations with or involvement in any organization or entity with any financial interest or non-financial interest in the subject matter or materials discussed in this manuscript.

## Acknowledgements

We would like to thank researchers in the field of archaeological science around the world, especially those who are dedicated to researching glass artifacts. Without their dedication and diligent efforts over the past decades, the outcomes of this study would not have been achievable. We gratefully acknowledge the valuable assistance provided by Junseop Oh, whose expertise in statistical analyses enhanced the rigor and depth of this research.

## Funding

This research was supported by grants from the National Research Foundation of Korea funded by the government (Grant number 2021R1A2C100601111).

## Author contributions

Conceptualization: B.C., S.-G.C., and Y.J.L.; Resources: B.K.L. and Y.J.; Methodology: B.C.; Formal analysis: B.C.; Investigation: B.C., J.S., S.K.C., and Y.J.; Data curation: B.C.; Visualization: B.C.; Writing-original draft: B.C.; Writing-review & editing: B.C., B.K.L., S.Y.L., and Y.J.L.; Project administration: Y.J.L.; Funding acquisition: Y.J.L.

## EarthArXiv Preprint

This manuscript is a non-peer reviewed preprint submitted to EarthArXiv. The content and structure may be modified prior to submission to a target journal for peer review.

## 1 Introduction

Food, clothing, and shelter—the basic necessities of life—are profoundly shaped by the climate and geology of the native region. In a similar vein, the products crafted inevitably bear the imprint of the nature. Glass, an artificial pre-modern material made from the fusion of natural raw materials, is one of the corresponding products. Nearly half a century ago, Sayre and Smith (1961) introduced the potential that compositional differences in ancient glass, and regional or chronological classifications were systematically interconnected. Despite ample opportunities for new interpretive approaches within a broader theoretical framework as subsequent analytical data accumulates (Rehren and Freestone 2015), their solid interpretations of the principal categories of ancient glasses remain unchallenged (Henderson 2013). Nevertheless, the underlying and reliable reason for the correlation remains unexplained. Decades later, since the interpretations were initially derived from the behavior of five pinpointing elements in approximately 200 fragments, thousands of glass analyses have accumulated due to the dedication of numerous researchers, and the advances in analytical techniques. The present moment presents an opportune occasion to unveil the concealed origins of ancient glass through novel insights from an interdisciplinary perspective, leveraging the definite geochemical fingerprints that a wider group of elements can tell us. Upon establishing these foundations, it will become feasible to elucidate the shape of bead trade and circulation on a global scale through examining the traces of ancient glasses scattered across the world.

In this study, we have compiled over two thousand chemical analyses of ancient glasses dating back to the pre-5th century CE, sourced from sixty-one academic references with openly available scientific data. Additionally, newly acquired glass bead data from the southern Korean Peninsula were incorporated to address data scarcity in this region. The geographical distribution of the data covers 128 localities in thirty-five countries across four continents. The chemical composition involved comprises thirty-eight elements, encompassing major, minor, and trace with rare-earth elements. Systematically organized data-based statistical processing enabled the differentiation of chemical glass types and the identification of their geo-spatiotemporal characteristics. Furthermore, an integrated exploration of the meaning within the geochemical signatures of each type was conducted, considering the perspective of climate and geology.

## 2 Materials and methods

### 2.1 Data collection and standardization

Geochemical data employed in this study mostly originated from peer-reviewed papers, complemented by materials gathered from several conference proceedings and books (ESM 2 Table S1). Individual literature was primarily obtained through academic online search services (e.g., google scholar), focusing on items highly ranked in resultant lists searched with associated keywords (e.g., ancient glass, glass beads, glass artifacts, chemical composition etc.). It is noted that there was no intentional bias during the collection process. For the Korean region's data, however, it constitutes a newly reported dataset in this study regarding the chemical properties of glass beads excavated from a twin tomb at Yeongam in the southern Korean Peninsula. Relevant backgrounds, data acquisition process, and results are described separately in ESM 1. Data collected from the literature includes the following items: chemical composition, place of discovery, period, color, method of analysis. Extraction of chemical analyses focused exclusively on reports for individual glass samples, excluding results presenting average values for certain groups due to the inability to compare them under uniform conditions. Owing to variations in reporting formats among different data sources authored by various individuals, specific data formats had to be converted to facilitate subsequent data processing and analyses: (1) the content of each element was converted into a metal-based value instead of an oxide form, (2) analytical results that were not detected (e.g., *n.d.* etc.) or indicated below the detection limits (e.g., *<dl*, *b.d.l.* etc.) were blanked only for the corresponding element, (3) color names were transformed into 6-digit hex color codes for standardization (ESM 2 Table S2), and (4) the age of artifacts, expressed as a period, was transformed into an arithmetic probability in centuries. For instance, when labeled as CE 400–500, 0.5 is assigned to both the 4th and 5th centuries.

Following the data collection process, a total of 6,865 glass analyses were acquired from sixty-one sources, including newly reported 57 results in this study. From these, 2,136 analyses meeting the specified criteria were selected as a final dataset for statistical analyses: (1) glass predating the 5th century, pertaining to the ancient time, (2) glass exhibiting distinct colors such as red, yellow, green, turquoise, blue, and colorless, and (3) glass containing no missing values for the seven major elements (Na, Mg, Al, Si, K, Ca, and Fe).

## **2.2 Statistical analyses**

Prepared glass dataset was investigated using both principal component analysis (PCA) and cluster analysis (CA) to categorize types of ancient glass and identify their geochemical characteristics. Prior to the statistical analyses, the dataset was split into the specified six color groups to ensure the independence of each analysis result from variations in glass colors. The processing of data on PCA and CA was performed using R Statistical Software for Windows (v4.1.3; R Core Team 2021). PCA is a statistical method used to reduce the dimensionality of complex variables, highlighting inter-relationships and sample variability among variables in multivariate datasets by exposing an underlying structure. In this study, seven variables representing major constituent elements (Na, Mg, Al, Si, K, Ca, and Fe) in 2,000+ glass samples were subjected to PCA to identify key factors influencing the classification of glass types globally. Given the compositional data characteristics of the variables, which represents parts of a whole, both log transformation and normalization were applied to all data values before employing PCA. The obtained loadings and scores were utilized to illustrate the relationship between variables and principal components (PCs) and to assess the extent to which each data sample reflects the extracted PCs.

CA is a statistical method that groups individual data points based on similarities (i.e., distance between data points), aiming to uncover intrinsic structures and patterns within a dataset. This study adopted  $k$ -means clustering algorithm, which minimizes within-cluster variances based on Euclidean distances as a criterion. Determining the optimal number of clusters ( $k$ ), a critical part of the analysis, was accomplished by applying the Hartigan index (Hartigan 1975). The classified clusters were displayed alongside PCA outcomes, featuring distinct colors for data points within each cluster.

## **3 Results**

### **3.1 Multivariate analyses: Confirmation of internal consistency**

Focused on the seven major elements, the combination of PCA and CA enabled the categorization of glass types into four distinct types (Fig. 1), except for two local variants. Table 1 presents representative statistical values of the elemental contents for each type and color of the glasses. Each classified type exhibits unique chemical characteristics setting it apart from others, while no statistical claim of absolute uniqueness is asserted.

In the context of PC loadings, a consistent pattern emerged across all glass colors, except for

**Table 1** Median concentration (in wt.%) of seven major elements, categorized by glass type and color, along with the interquartile range (in gray color).

<b>Type</b>	<b>Color</b>	<b>n</b>	<b>Na</b>	<b>Mg</b>	<b>Al</b>	<b>Si</b>	<b>K</b>	<b>Ca</b>	<b>Fe</b>
Na-Mg	Yellow	49	12.15 (10.29–12.98)	2.35 (1.94–2.88)	0.64 (0.46–0.85)	30.53 (28.19–31.60)	1.92 (1.32–2.47)	4.80 (3.62–5.40)	0.45 (0.26–0.83)
	Green	164	12.31 (11.13–13.80)	2.43 (2.04–2.88)	0.85 (0.56–1.28)	29.64 (28.13–31.43)	2.37 (1.44–2.82)	4.51 (3.76–5.30)	0.48 (0.30–0.76)
	Turquoise	124	12.53 (10.80–13.50)	2.58 (2.10–3.18)	0.59 (0.36–0.79)	30.20 (29.22–31.29)	2.29 (1.64–2.68)	4.29 (3.94–5.47)	0.42 (0.27–0.56)
	Blue	127	12.86 (11.47–13.81)	2.73 (2.27–3.15)	0.56 (0.44–0.92)	29.96 (28.84–31.10)	2.44 (1.73–2.91)	4.49 (3.91–5.09)	0.48 (0.30–0.58)
	Colorless	37	12.31 (11.77–13.43)	2.35 (1.95–2.89)	0.48 (0.34–0.59)	30.82 (29.97–32.22)	1.67 (1.01–2.49)	5.07 (4.00–5.70)	0.31 (0.24–0.51)
Na-Ca	Red	41	10.91 (9.86–13.09)	0.65 (0.33–1.42)	1.24 (0.96–1.44)	28.21 (25.93–30.48)	0.96 (0.51–1.84)	5.53 (4.48–6.29)	0.94 (0.47–1.28)
	Yellow	85	10.07 (8.19–13.14)	0.27 (0.21–0.37)	1.03 (0.63–1.24)	28.20 (24.45–31.03)	0.47 (0.24–0.57)	4.37 (3.14–4.92)	0.87 (0.41–1.12)
	Green	148	12.79 (11.82–13.35)	0.36 (0.33–0.48)	1.24 (1.16–1.34)	32.19 (30.72–32.70)	0.46 (0.38–0.52)	4.87 (4.43–5.61)	0.39 (0.33–0.60)
	Turquoise	148	12.06 (10.05–13.30)	0.31 (0.24–0.48)	1.54 (1.15–3.39)	31.26 (28.88–32.30)	0.56 (0.39–1.34)	3.79 (1.71–5.56)	0.56 (0.34–0.82)
	Blue	366	12.39 (11.73–13.27)	0.36 (0.30–0.44)	1.26 (1.16–1.37)	32.30 (31.24–32.87)	0.46 (0.36–0.60)	5.07 (4.30–5.68)	0.54 (0.34–0.89)
	Colorless	120	13.06 (11.97–13.85)	0.34 (0.29–0.46)	1.26 (1.10–1.39)	31.87 (31.03–32.63)	0.54 (0.38–0.67)	5.27 (4.27–5.86)	0.30 (0.23–0.50)
Na-Al	Red	99	9.40 (7.97–12.08)	0.91 (0.52–1.03)	3.74 (3.25–4.37)	29.92 (28.83–31.72)	2.99 (2.15–3.89)	2.24 (1.84–3.07)	1.02 (0.80–1.62)
	Yellow	60	11.89 (10.56–13.38)	0.20 (0.19–0.26)	4.54 (4.06–6.79)	27.38 (26.12–30.05)	1.55 (0.71–2.01)	1.69 (1.47–1.84)	0.95 (0.73–1.41)
	Green	85	11.42 (8.38–12.44)	0.41 (0.22–0.72)	4.05 (3.04–5.75)	28.98 (28.19–31.18)	1.78 (1.34–2.39)	1.81 (1.55–2.75)	1.05 (0.89–1.39)
	Blue	122	5.00 (2.38–12.08)	0.21 (0.07–0.35)	4.37 (2.32–5.79)	29.48 (28.36–31.66)	2.11 (1.13–3.64)	1.42 (1.07–6.68)	0.61 (0.42–0.88)
K	Red	19	0.98 (0.38–1.11)	1.84 (1.69–2.16)	1.58 (1.43–1.63)	28.14 (27.77–30.06)	14.36 (12.99–15.69)	4.17 (3.52–4.85)	1.40 (1.04–1.68)
	Yellow	19	0.16 (0.13–0.28)	0.10 (0.08–0.20)	1.58 (1.00–6.99)	22.39 (17.03–23.64)	7.47 (0.50–9.25)	0.39 (0.27–1.12)	0.99 (0.77–4.80)
	Green	21	0.75 (0.40–0.84)	0.27 (0.12–0.39)	1.40 (1.01–2.10)	34.08 (32.26–35.76)	12.95 (11.12–14.72)	1.11 (0.55–1.99)	0.45 (0.41–0.64)
	Turquoise	109	1.07 (0.42–3.39)	0.28 (0.18–0.39)	1.15 (0.87–1.55)	35.11 (34.30–36.51)	10.63 (7.80–12.69)	1.50 (0.95–1.97)	0.42 (0.29–0.57)
	Blue	152	0.43 (0.15–0.69)	0.26 (0.15–0.43)	1.52 (1.12–2.19)	34.73 (33.58–35.77)	12.95 (11.06–13.93)	1.23 (0.67–1.91)	0.83 (0.64–1.04)
	Colorless	14	0.41 (0.25–0.47)	0.13 (0.08–0.24)	0.75 (0.59–1.76)	36.97 (36.03–37.50)	12.87 (12.04–13.78)	1.10 (0.93–1.84)	0.55 (0.28–0.59)
Fe	Red	12	0.77 (0.42–1.28)	0.18 (0.14–0.23)	1.05 (0.94–1.56)	15.77 (14.04–16.61)	0.61 (0.33–0.93)	1.63 (1.33–1.99)	14.60 (11.67–24.21)
Ca-Al	Colorless	15	3.33 (2.43–4.19)	0.03 (0.02–0.04)	6.97 (6.85–7.18)	29.09 (28.56–29.84)	2.91 (1.41–3.67)	10.91 (9.82–11.87)	0.35 (0.28–0.42)

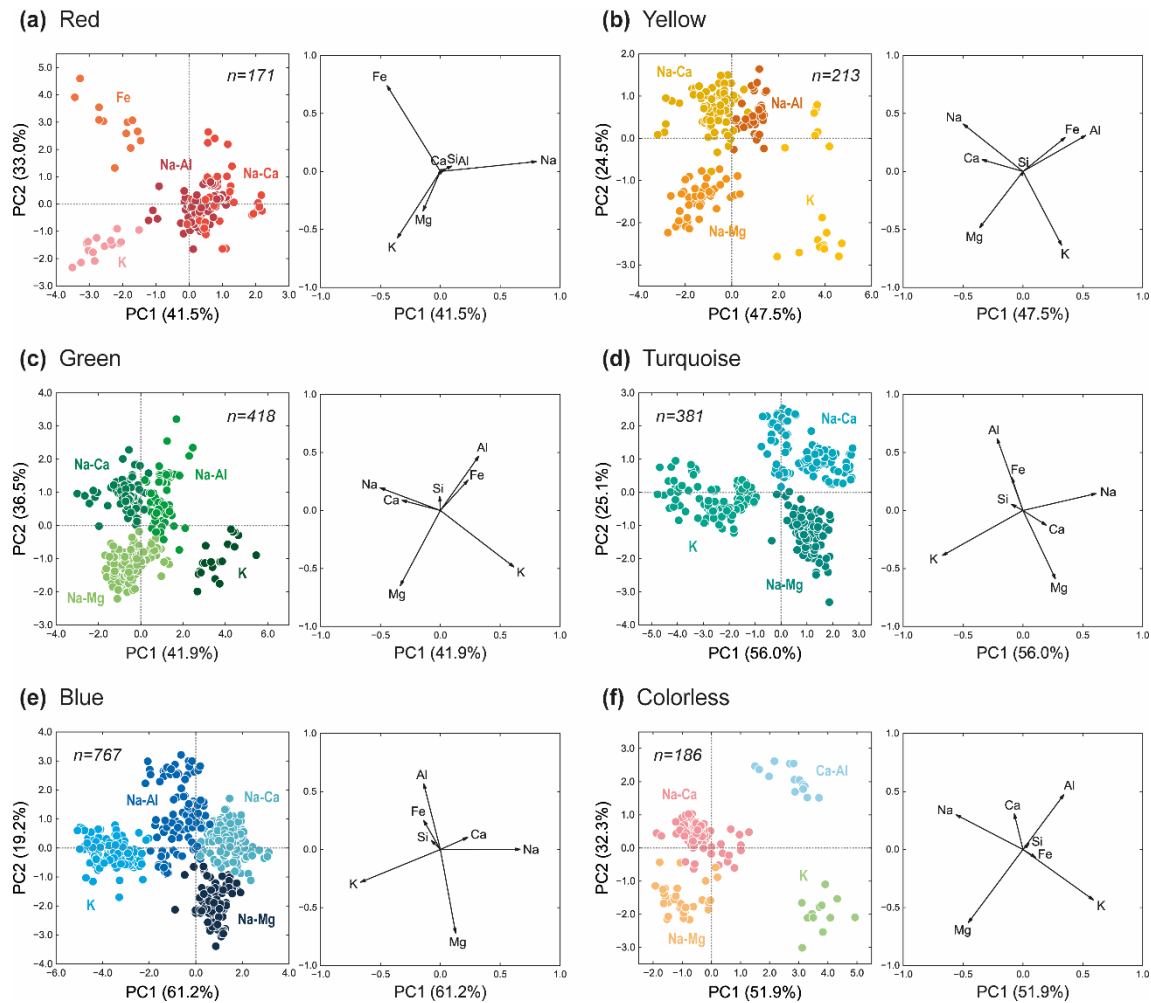


**Fig. 1** Bivariate plots of principal component (PC) scores and loadings for ancient glass data by color. Clusters of ancient glass, categorized by color through *k*-means cluster analysis, are represented on the PC score plane.

the extraordinary red. The loadings associated with Na, K, Al, and Mg display a radial orientation in four distinct directions, forming approximate right angles (Fig. 1). These arrangements imply that each element acts as an incompatible end member with distinct characteristics from the others. Indeed, these elements are fundamentally connected to the fluxes' properties (e.g., biogenic or geogenic origins) utilized in glass production and to the underlying climatic and geological conditions. Their roles are pivotal in differentiating the geochemical signatures of clusters identified through CA. Additionally, it is observed that the loadings of two specific elements exhibit a concurrent directional movement. Specifically, the presence of Al–Fe and Na–Ca pairs are present, and although there are variations in magnitude depending on the color of the glass, a clear trend can be discerned (Fig. 1). There are definitive reasons for these

consistent geochemical traits, and we aim to elucidate the inevitability of such characteristics within the context of sequential processes in environments where climate and geology are interlinked. Further details are elaborated upon subsequently.

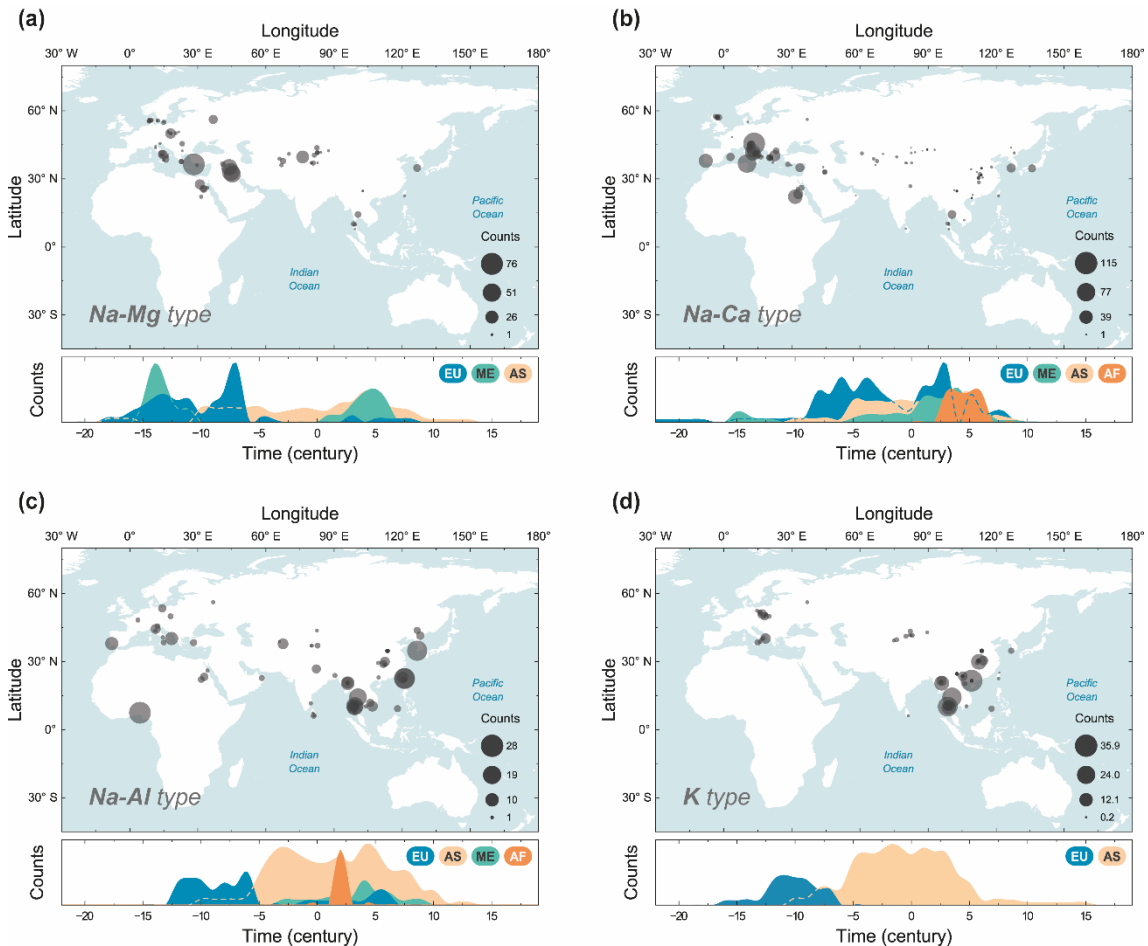


**Fig. 2** Spatiotemporal distribution and frequency of occurrence for ancient glass by classified type. The vertical axis of time series data corresponds to square root scale. EU = Europe, AS = Asia, ME = Middle East, and AF = Africa.

### 3.2 Distinct geochemistry in glass types yields unique spatiotemporal distribution

Geospatial and temporal visualization of glasses showed discernible differences based on the classified types (Fig. 2). Nonetheless, even within the same category, the processes of production, circulation, utilization, and final deposition vary, leading to a broad geographic spread of glass artifacts, as illustrated on the map. In the first instance, Na-Mg type glass aligns with the commonly referred ‘plant ash glass’, which is a typical soda-lime glass with a high magnesium content (Table 1). It is predominantly found in



the historical “cradle of civilization”, comprising the Middle East and Egypt, and extends from the Balkans to the southern part of the Apennine Peninsula and to Denmark through Eastern Europe, with some occurrences in parts of Asia (Fig. 2a). In terms of the time series, its peak prosperity spanned from approximately 1,500 to 700 BCE, except for a recession during the Greek Dark Ages (circa 1,100–800 BCE).

The second type, Na-Ca glass, is known as ‘natron glass’, which utilizes sodium carbonates (e.g., natron, trona) as a fluxing agent. This type has lower levels of potassium and magnesium compared to the former, but a higher amount of aluminum (Table 1), indicative of a mineral origin for bulky source materials. As the power shifts from Mesopotamia to Europe, the density of glass decreases in the Fertile Crescent while increasing in regions along the southern coast of the Anatolian Peninsula, extending towards southern Europe and North Africa (Fig. 2b). Although in limited amounts, its presence is also confirmed along the Asian inland route to the Indochina Peninsula and Far East Asia. Their golden age substantially coincides with the rise and fall of Rome, spanning from the Roman Kingdom in the 8th century BCE through the Republican and Imperial periods until the division into the Eastern and Western Empires in the late 4th century CE.

The third chemical category is Na-Al type, characterized by more than double the aluminum content and considerable variability in sodium composition within different color groups (Table 1). The composition seems to align with the ‘Indo-Pacific glass’ category (Francis 1988; Dussubieux et al. 2010; Pion and Gratuze 2016). While the majority occurs in the Far East including Southeast Asia, the geospatial bias is minimal due to significant quantities also found in Europe, Middle East, Africa, and Central Asia (Fig. 2c). Given its tendency to generally distribute along coastlines (e.g., the Mediterranean Sea, and spanning from the Bay of Bengal up to the Yellow Sea), the extensive geographical prevalence appears to originate from a principal reliance on maritime trade (Francis 2002). This type held dominance exclusively within Europe during approximately the 13th–5th centuries BCE. Subsequently, a clear bimodal distribution has emerged, primarily shifting the center of influence to Asian regions. The context and reason for the bimodality have not been established yet.

Lastly, K type glass contains potassium as a primary constituent after silica and, in certain instances, exhibits comparable proportions to sodium. Potassium content usually exceeds 10 wt.% on average, while the other five major elements remain below 2 wt.% (Table 1). This category covers the

listed four traditional glass types, forming a unified group owing to their relatively coherent composition: (1) high potassium glass (HKG), (2) low magnesium and high potassium (LMHK) glass, and (3) mixed-alkali glass in Europe, (4) potash glass in Asia. The origin of these potassium-rich glasses remains uncertain (Liu et al. 2013; Dussubieux et al. 2020; Ma et al. 2022a). However, the compiled geographical distribution suggests a confined potential provenance. The highest spatial density is observed along the line from the Malay Peninsula to the eastern inland China, to a lesser degree in southern Italy and Poland, as well as in some parts of the Central Asian Silk Road (Fig. 2d). Like the prior Na-Al type, its chronological distribution is divided into a dominant European era preceding the circa 7th–6th centuries BCE, followed by an Asian predominance, with some temporal overlap. Once more, the implications of this bimodality are still uncertain.

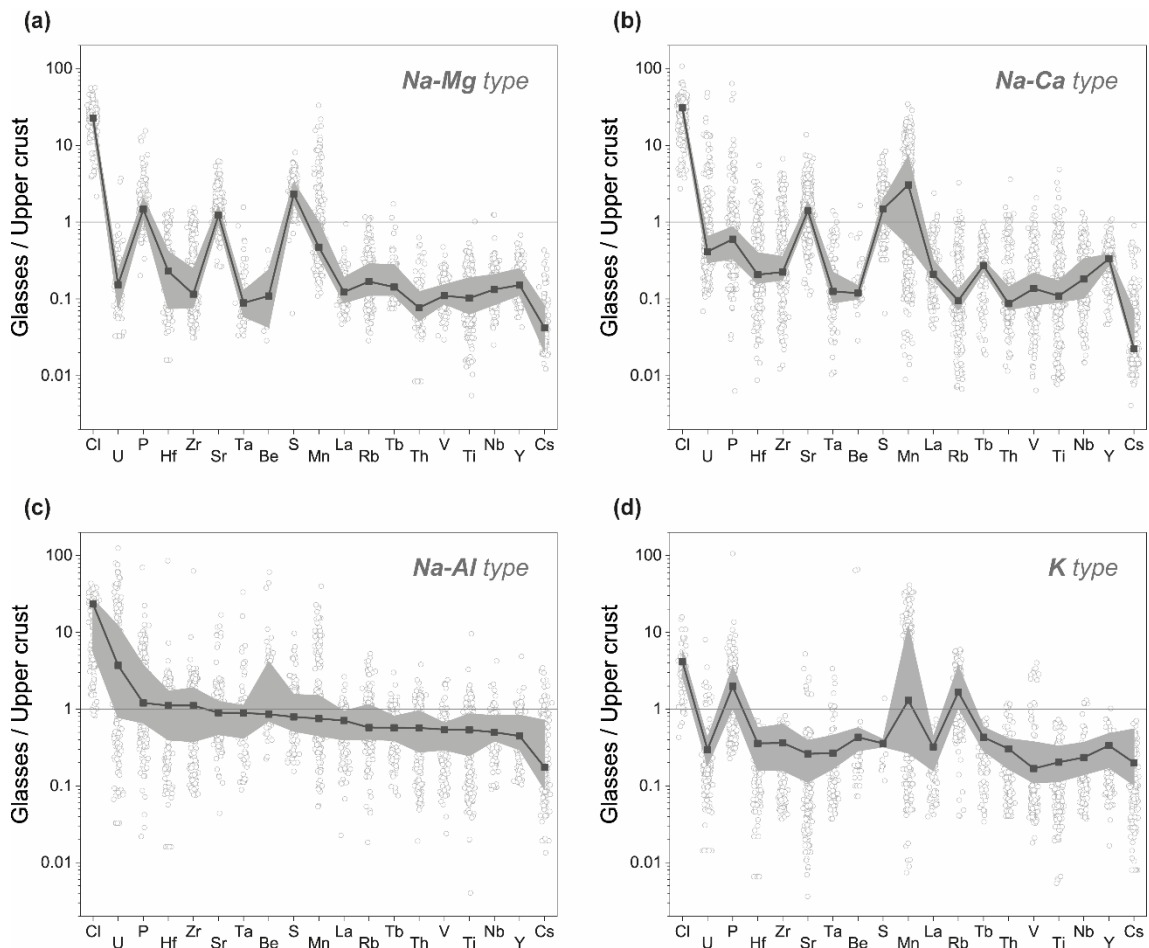


**Fig. 3** Sequential variational patterns of minor and trace elements by classified type. Glass data are normalized to the composition of upper crust (Rudnick and Gao 2014). Solid line denotes the median, while the gray area represents the interquartile range. Open circles in the background correspond to individual data.

## **4 Discussion**

### ***4.1 Climate and geology shape glass compositions through raw material selection***

The presence of glass types distinguished by an independent singularity in terms of chemistry, geography, and time span highlights its originality. In this regard, regions with a high occurrence density of a particular glass type likely indicate comprehensive centers for producing and distributing that glass, implying potential provenance in a broad sense. Simultaneously, it is essential to note that the geographic scope itself is intertwined with unique climatic and geological characteristics, which impact the physiochemical and mineralogical attributes of raw materials employed in glassmaking significantly. Consequently, a given glass type could display distinct patterns of minor and trace elements resembling fingerprints, thereby providing insights into the provenance and source of the raw materials (Fig. 3).

### ***4.2 Carbonate legacy: Across the Mediterranean to the Middle East***

In the Mediterranean Sea and its coastal regions, calcareous geological formations are ubiquitous (Laugié et al. 2019; Michel et al. 2019). This is closely linked to the evolution of the ancient Tethys Sea and its associated tectonics since the Mesozoic Era (Calvo and Regueiro 2010). During periods of extensional tectonic regime (e.g., passive continental margins) in the Mesozoic and Neogene, widespread carbonate platforms with bioclastic sediments (e.g., remains of stony corals and seashells) developed in shallow and warm marine basins alongside the Tethys, particularly ranging from the Mediterranean to the Middle East (Michel et al. 2020). These rocks then uplifted mainly during the Pliocene, culminating in their current state. Hence, it is logical that the distribution of the Na-Mg and Na-Ca types, marked by a notable calcium content of approximately 4–5 wt.% (Table 1) and a prominent positive strontium (Sr) anomaly (Fig. 3a, b), centers on the Mediterranean and Middle East regions. In general, substitution of calcium ions for strontium ions exhibits a higher affinity for aragonite, a major constituent mineral of the bioclastic sediments, than for calcite due to differences in their inherent crystallographic compatibility (Finch and Allison 2007).

### ***4.3 Mid-latitude high-pressure zone: Saline lakes with evaporites***

Climate also engaged with geology as an influential factor. Paleolatitude reconstruction reveals that the Mediterranean region shifted northward over the past 50 million years, spanning approximately 20–35° N

(Besse and Courtillot 2002; Torsvik et al. 2012; van Hinsbergen et al. 2015). These latitudes, corresponding to the mid-latitudinal high-pressure zone, features descending air masses induced by the latitudinal atmospheric circulation near the 30th parallel. The masses suppress vertical cloud development and subsequent rain formation, resulting in arid and semi-arid climates. This leads to more evapotranspiration relative to annual precipitation and facilitates the formation of saline lakes with accompanying evaporites (e.g., gypsum, halite) in the Mediterranean Basin and along the Red Sea coast. Like strontium (Sr), a sulfur (S) peak is evident in both Na-Mg and Na-Ca types (Fig. 3a, b). These sulfur anomalies are expected to originate from inorganic sulfur, particularly the widespread gypsum (Natalicchio et al. 2014). Sulfur from organic sources, such as halophytes, may also be present, but it is likely that it has already been volatilized in the high-temperature environment during plant ashing (e.g., Barlow 1904; Jackson et al. 2005). Meanwhile, strontium substitution can also take place in gypsum, but less common and generally occurs in trace amounts compared to carbonates mentioned above.

The precipitation of sodium carbonate is another consideration in the context of the evaporitic environment, as it necessitates the influx of a highly alkaline source beyond the evaporitic setting. The alkaline composition typically sources from alkali-rich rocks and minerals (e.g., carbonatite, nephelinite, phonolite, and melilite), primarily associated with alkaline magmatism found in continental rifts and intraplate hotspots (Philpotts and Ague 2022). Near the Middle East, the East African Rift stands as the world's largest active continental rift zone, featuring a volcanic composition that spans from hyperalkaline to tholeiitic and felsic rocks (Saemundsson 2010). In this zone, one can find Ol Doinyo Lengai, the only active volcano on Earth associated with natrocarbonatitic lava eruption. To the north of the volcano lies Lake Natron, characterized by its high sodium carbonate content, and the area affected by volcanic eruptions substantially coincides with the upper Nile River basin. This suggests that the alkaline-rich sources from large-scale eruptions could migrate enough downstream along the river. Such geological and geographical peculiarities substantiate Egypt's pivotal role as a natron supplier, as confirmed by historical literature (Conte et al. 2016; Jackson et al. 2018).

Previous discussions have confirmed that Na-Mg and Na-Ca glass types originate from similar geological and climatic settings, yet the Mg content is significantly higher in the Na-Mg type (Table 1). Fundamental distinction arises from the type of flux utilized: Na-Mg glass is produced using biogenic flux from the ash of halophytes in saline environments, unlike the geogenic flux in Na-Ca glass, which is

the primary factor for the Mg content discrepancy. Specifically, in saline lake contexts where halophytes thrive, the precipitation of Ca carbonate leads to a reduction in  $\text{Ca}^{2+}$  concentration, commonly resulting in an increased Mg/Ca ratio, which may facilitate the formation of Mg carbonate (Eugster and Hardie 1978; Tosca and Tutolo 2023). While there is variability among halophyte species, ash commonly contains significant MgO content, typically within the range of 2 to 10 wt.% (Henderson 2013). This evidence reduces the probability that the elevated Mg content in Na-Mg glass is due to the enhanced use of stony coral and seashell fragments.

#### ***4.4 Tropical weathering processes: Upper crust-like compositions***

On the contrary, the Na-Al type displays an almost flat pattern with y-values near unity in the multi-element diagram (Fig. 3c), signifying a pronounced chemical similarity between this glass type and the Earth's upper crust. The diagram predominantly features elements categorized as incompatible, and they are relatively abundant in the upper crust. In the K type, albeit to a lesser extent, it demonstrates an overall pattern and elemental content akin to the Na-Al type, except for specific anomalies in P, Mn, and Rb (Fig. 3d). Certainly, it bears much lower similarity to the Na-Mg and Na-Ca types.

These two glasses (i.e., Na-Al and K types) are mainly found in the Asian region, with the highest density observed in Southeast Asia, centered around the Indochina Peninsula (Fig. 2c, d). The region, extending from India through the peninsula to inland eastern China, has a tropical climate (including monsoon and savanna patterns) along with a humid subtropical climate (Peel et al. 2007), marked by high average temperature, annual precipitation, and alternating dry and wet seasons. These climatic conditions expedite the weathering and erosion of prevalent granitic rocks in the continental crust. This process releases incompatible elements into soils and surface waters, resulting in their enrichment in the uppermost layers of the Earth's crust. Specifically, tropical weathering processes, such as laterization, lead to intense leaching, causing the removal of soluble elements. Nevertheless, certain elements such as Fe, Al, Ti, Mn, V and Ni exhibit notable resistance to leaching and remain in the soil, contributing to laterite formation. As presented in Table 1, the consistently high aluminum and iron content in the Na-Al type, regardless of glass color, is attributed to the utilization of raw materials that reflect the regional climate and geological characteristics, thus confirming their provenance. This also suggests the incorporation of highly weathered sources in the raw materials like soils or its derivatives. A

representative example is sodic efflorescence called reh (Agrawal and Gupta 1968; Brill 1987; Dussubieux et al. 2010), which served as a flux in the production of Indo-Pacific beads of the Na-Al type. Uniquely, both reh and laterite formation share the characteristic of rainwater percolation into surficial rocks as well as leachate rise driven by capillary action recurring during alternating wet and dry seasons (Wadia 1975; Dussubieux et al. 2022).

In particular, K type glass is posited to originate from regions devoid of geogenic mineral fluxes and halophytes. Its distribution predominantly covers the region from the interior of the Indochina Peninsula to southern mainland China (Fig. 2d), marked by extensive vegetation and tropical rainforests. As a result, an ash-based flux like that used in Na-Mg glass was adopted; however, wood ash was utilized, manifesting unique geochemical signatures. Furthermore, a pronounced positive anomaly in Rb, which easily substitutes for K, is identified as a defining trait of K type glass (Fig. 3d). These factors underscore the significant influence of climate and the geological attributes of raw materials in the origin identification.

#### ***4.5 Phosphorus and manganese: From fluxes to orogenic belts***

Patterns of minor and trace elements also provide insights into estimating the origin of flux. For instance, an anomalous phosphorus signal could indicate the use of biogenic-origin flux like plant ash in glass manufacturing (Stern 2017). This is because phosphate plays a pivotal role in the framework formation of both flora and fauna and remains resistant to decomposition at high temperatures. As a result, it persists in the residual ash, imparting a distinctive chemical signature to the glass in which it is employed. Indeed, positive phosphorus anomalies are evident in the Na-Mg and K types (Fig. 3a, d), indicating the use of plant or wood ash, in line with previous research findings. In contrast, Na-Ca and Na-Al types, denoting glasses produced with geogenic-origin flux such as natron and reh, exhibited either no peak or only minimal levels (Fig. 3b, c). A noteworthy observation is that the absolute phosphorus content in the Na-Al type closely resembles that of the Na-Mg and K types (Fig. 3), without any conspicuous peaks. This occurrence is likely due to the prevalence of phosphate minerals (e.g., monazite and xenotime) associated with REE deposits in this region, rather than to biogenic sources, as will be elaborated on later.

Regarding manganese, spikes and large deviations are only evident in the Na-Ca and K types (Fig. 3b, d), which are based in Europe and Southeast Asia, respectively. This behavior is especially

prominent in the Alps (northern Italy) and the Eastern Himalayan Fold Belt region centered on Myanmar. Both these regions share the characteristic of being located within global orogenic belts associated with Jurassic–Cretaceous ophiolites (Saccani 2015). The connection between ophiolites and manganese is primarily related to the presence of manganese-rich deep marine sediments or associated rocks in the uppermost part of the ophiolite complex. Upon the uplift of these complexes, subsequent weathering and concentration processes lead to the development of ore deposits or nodules in its vicinity. Nonetheless, manganese solubility is influenced by an intricate interplay of factors including the ion’s oxidation state, pH, redox conditions, and its complexation. Consequently, manganese concentration shows substantial spatial heterogeneity, which explains the large deviations observed in the glass analyses.

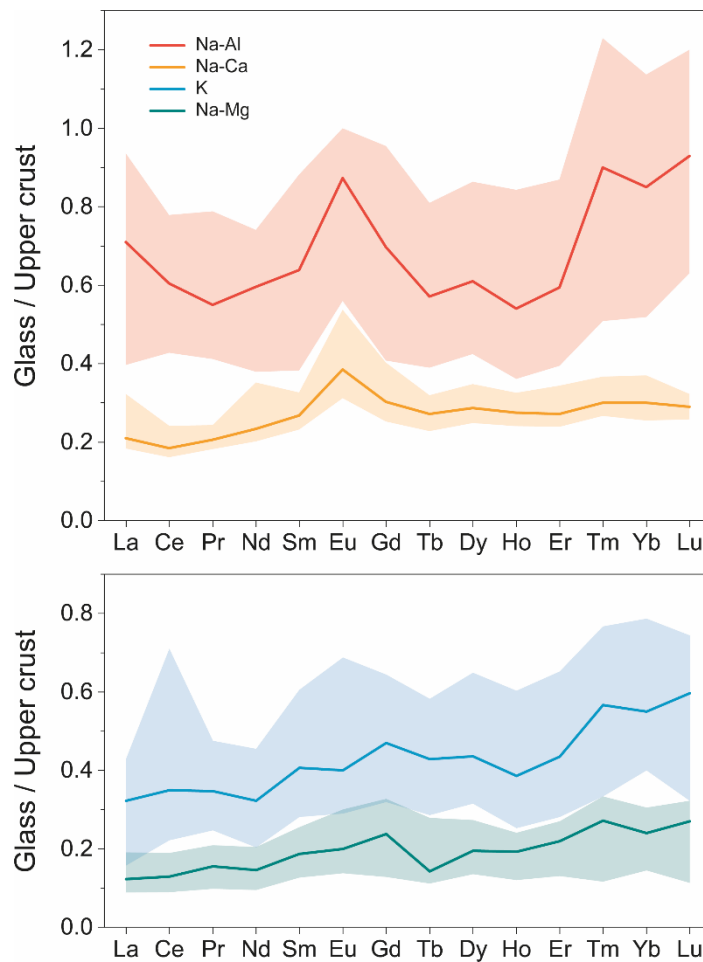


**Fig. 4** Upper crust-normalized rare-earth element patterns for different glass types. Normalizing values from Rudnick and Gao (2014). Solid line denotes the median, while the gray area represents the interquartile range.

#### **4.6 Rare-earth element (REE): Core repository for cross-check**

A clear contrast in the occurrence of REE deposits between Europe–Middle East and Asia provides an enhanced foundation for more robust provenance identification. Although rare in Europe and the Middle East, numerous deposits are either under development or identified across Asia, extending from India through Southeast Asia to northeastern China, with a fairly even spatial distribution (Deady 2021). The normalized REE patterns for each glass type demonstrate these characteristics well (Fig. 4). The Na-Al and K types, predominantly found in Asia, present higher REE levels compared to the Na-Ca and Na-Mg types prevalent in Europe and the Middle East, respectively. Furthermore, the clear recognition of heavy REE enrichment, which can be considered a signature of REE deposits in Asia (Xie et al. 2016; Li et al. 2017), in both Na-Al and K types of patterns indicates the utilization of local source materials reflecting the regional geology. Final point to note is the presence of a positive europium (Eu) anomaly, observed in both Na-Al and Na-Ca types (Fig. 4). In general, divalent europium ( $\text{Eu}^{2+}$ ) is known to preferentially incorporate into plagioclase in reducing magma due to its ion size and charge similarity with the  $\text{Ca}^{2+}$  ion of plagioclase. Accordingly, a positive Eu anomaly indicates the presence of plagioclase in the source materials. Coincidentally, both glass types correspond to cases where geogenic-origin flux was utilized, implying inadvertent introduction of plagioclase along with fluxes into the glassmaking process. Notably, the Eu anomaly is most pronounced in the Na-Al type, which is prone to incorporating weathered soil due to regional climatic conditions. On the other side, feldspar often shares grain boundaries with quartz in rocks, potentially leading to its unintentional inclusion as a raw material. However, considering that the Eu anomaly is prevalent only in types primarily reliant on geological-origin fluxes, it can be inferred that the quartz used was in a pure state with minimal impurities.

## **5 Conclusions**

Utilizing over 2,000 chemical analysis datasets gathered during this study, ancient glass artifacts have been categorized into several distinct types based on their major chemical compositions. The origins, as well as the geospatial and temporal distribution characteristics, of the unique geochemical properties of each type, have been analyzed from both climatic and geological perspectives. Naturally, given that the dataset does not encompass all available glass analyses, it remains a possibility that the robustness of the interpretation could undergo slight variations with the inclusion of additional data. Furthermore, it is



conceivable that certain individual glass samples may exhibit characteristics of multiple types simultaneously or possess more nuanced subtypes, potentially introducing classification ambiguity. Nevertheless, the study's key findings entail the classification of four unique types of ancient glasses using objective statistical techniques. Moreover, it highlights that the chemical fingerprints of each type are inherently linked to geography, geology, and climate, confirming their interdependence.

In the future, efforts should focus on a comprehensive interpretation that integrates the geochemical approach with typology, while also considering the social, economic, and ritual uses of glass. It is also imperative to investigate the evolution of glass across an extended temporal and spatial context, encompassing the medieval and modern eras beyond ancient times. Notably, there is a pressing need to expand glass analysis data in the Indian region, a geographically significant area bridging Europe and Southeast Asia. Above all, the paramount importance lies in providing novel insights to reconstruct the development patterns of trade and circulation of glass artifacts based on scientific data rather than relying only on literature. From this perspective, the spatiotemporal distribution data enable us to infer the glass's origin but also serve as a representation of a distribution network by offering insights into its movement, utilization, and eventual burial. The picture will become clearer with the accumulation of additional data. Lastly, the discovery of various types of ancient glass in Korea holds significance as it confirms Korea's active participation in global trade at the time, despite its location at the eastern end of the Eurasian continent.

**Supplementary information** This study includes two supplementary materials and details are described below.

- 1) Electronic Supplementary Material 1 (ESM 1): Materials and methods
- 2) Electronic Supplementary Material 2 (ESM 2): Tables S1 to S6

**Acknowledgements** We would like to thank researchers in the field of archaeological science around the world, especially those who are dedicated to researching glass artifacts. Without their dedication and diligent efforts over the past decades, the outcomes of this study would not have been achievable. We gratefully acknowledge the valuable assistance provided by Junseop Oh, whose expertise in statistical analyses enhanced the rigor and depth of this research.

**Author contributions** Conceptualization: B.C., S.-G.C., and Y.J.L.; Resources: B.K.L. and Y.J.; Methodology: B.C.; Formal analysis: B.C.; Investigation: B.C., J.S., S.K.C., and Y.J.; Data curation: B.C.; Visualization: B.C.; Writing-original draft: B.C.; Writing-review & editing: B.C., B.K.L., S.Y.L., and Y.J.L.; Project administration: Y.J.L.; Funding acquisition: Y.J.L.

**Funding** This work was supported by grants from the National Research Foundation of Korea funded by the government (grant number 2021R1A2C100601111).

**Data availability** The original contributions and data sources used in the study are given in the article and supplementary materials.

**Code availability** Not applicable.

## **Declarations**

**Ethics approval** Not applicable.

**Consent to participate** Not applicable.

**Consent for publication** Not applicable.

**Competing interests** The authors declare no competing interests.

## References

- Abdurazakov AA (2009) Central Asian glassmaking during the ancient and medieval periods. In: Fuxi G, Brill RH, Shouyun T (eds) *Ancient glass research along the Silk Road*. World Scientific, pp 201–219.
- Agrawal RR, Gupta RN (1968) Saline-alkali soils in India. *Technical Bulletin (Agric.) Series*, vol. 15. Indian Council of Agricultural Research, New Delhi.
- Arletti R, Bertoni E, Vezzadini G, Mengoli D (2011) Glass beads from Villanovian excavations in Bologna (Italy): an archaeometrical investigation. *Eur. J. Mineral.* 23(6):959–968.  
<https://doi.org/10.1127/0935-1221/2011/0023-2166>
- Babalola AB, Dussubieux L, McIntosh SK, Rehren T (2018) Chemical analysis of glass beads from Igbo Olokun, Ile-Ife (SW Nigeria): New light on raw materials, production, and interregional interactions. *J. Archaeol. Sci.* 90:92–105. <https://doi.org/10.1016/j.jas.2017.12.005>
- Barlow WE (1904) On the losses of sulphur in charring and in ashing plant substances and on the accurate determination of sulphur in organic substances. *J. Am. Chem. Soc.* 26(4):341–367.
- Bertini M, Shortland A, Milek K, Krupp EM (2011) Investigation of Iron Age north-eastern Scottish glass beads using element analysis with LA-ICP-MS. *J. Archaeol. Sci.* 38(10):2750–2766.  
<https://doi.org/10.1016/j.jas.2011.06.019>
- Besse J, Courtillot V (2002) Apparent and true polar wander and the geometry of the geomagnetic field over the last 200 Myr. *J. Geophys. Res. Solid Earth* 107(B11):EPM 6-1–31.  
<https://doi.org/10.1029/2000JB000050>
- Blomme A, Degryse P, Dotsika E, Ignatiadou D, Longinelli A, Silvestri A (2017) Provenance of polychrome and colourless 8th–4th century BC glass from Pieria, Greece: a chemical and isotopic approach. *J. Archaeol. Sci.* 78:134–146. <https://doi.org/10.1016/j.jas.2016.12.003>
- Brill RH (1987) Chemical analyses of some early Indian glasses. In: Bhardwaj HC (ed.) *Archaeometry of glass—proceedings of the archaeometry session of the XIV International Congress on Glass—1986*. Indian Ceramic Society, pp 1–25.
- Brill RH (2009) Opening remarks and setting the stage: lecture at the 2005 Shanghai International Workshop on the archaeology of glass along the Silk Road. In: Fuxi G, Brill RH, Shouyun T (eds) *Ancient glass research along the Silk Road*. World Scientific, pp 109–147.

- Calvo JP, Regueiro M (2010) Carbonate rocks in the Mediterranean region—from classical to innovative uses of building stone. *Geol. Soc. Lond. Spec. Publ.* 331(1):27–35. <https://doi.org/10.1144/SP331.3>
- Conte S, Arletti R, Mermati F, Gratuze B (2016) Unravelling the Iron Age glass trade in southern Italy: the first trace-element analyses. *Eur. J. Mineral.* 28(2):409–433. <https://doi.org/10.1127/ejm/2016/0028-2516>
- Conte S, Matarese I, Vezzalini G, Pacciarelli M, Scarano T, Vanzetti A, Gratuze B, Arletti R (2019) How much is known about glassy materials in Bronze and Iron Age Italy? New data and general overview. *Archaeol. Anthropol. Sci.* 11:1813–1841. <https://doi.org/10.1007/s12520-018-0634-6>
- Costa M, Barrulas P, Arruda AM, Dias L, Barbosa R, Vandenaabeele P, Mirão J (2021) An insight into the provenance of the Phoenician-Punic glass beads of the necropolis of Vinha das Calças (Beja, Portugal). *Archaeol. Anthropol. Sci.* 13(9):149. <https://doi.org/10.1007/s12520-021-01390-5>
- Deady E (2021) Global rare earth element (REE) mines, deposits, and occurrences (May 2021). British Geological Survey. [https://www2.bgs.ac.uk/mineralsuk/download/global\\_critical\\_metal\\_deposit\\_maps/G2122\\_022\\_V6R\\_GB.pdf](https://www2.bgs.ac.uk/mineralsuk/download/global_critical_metal_deposit_maps/G2122_022_V6R_GB.pdf)
- Degryse P, Boyce A, Erb-Satullo N, Eremin K, Kirk S, Scott R, Shortland AJ, Schneider J, Walton M (2010) Isotopic discriminants between late Bronze Age glasses from Egypt and the Near East. *Archaeometry*, 52(3):380–388. <https://doi.org/10.1111/j.1475-4754.2009.00487.x>
- Dong JQ, Li QH, Liu S (2015) The native development of ancient Chinese glassmaking: a case study on some early lead–barium–silicate glasses using a portable XRF spectrometer. *X-Ray Spectrom.* 44(6):458–467. <https://doi.org/10.1002/xrs.2651>
- Dupree L, Angel JL, Brill RH, Caley ER, Davis RS, Kolb CC, Marshack A, Perkins D, Solem A (1972) Prehistoric research in Afghanistan (1959-1966). *Trans. Am. Philos. Soc.* 62(4):1–84. <https://doi.org/10.2307/1005969>
- Dussubieux L, Bellina B (2018) Glass ornament production and trade polities in the Upper-Thai Peninsula during the Early Iron Age. *Archaeol. Res. Asia* 13:25–36. <https://doi.org/10.1016/j.ara.2017.08.001>
- Dussubieux L, Bellina B, Oo WH, Win UMS, Tut HM, Htwe KMM, Kyaw K (2020) First elemental analysis of glass from Southern Myanmar: replacing the region in the early Maritime Silk Road.

- Archaeol. Anthropol. Sci. 12:139. <https://doi.org/10.1007/s12520-020-01095-1>
- Dussubieux L, Fenn TR, Abraham SA, Kanungo AK (2022) Tracking ancient glass production in India: elemental and isotopic analysis of raw materials. *Archaeol. Anthropol. Sci.* 14(12):226. <https://doi.org/10.1007/s12520-022-01692-2>
- Dussubieux L, Gratuze B, Blet-Lemarquand M (2010) Mineral soda alumina glass: occurrence and meaning. *J. Archaeol. Sci.* 37(7):1646–1655. <https://doi.org/10.1016/j.jas.2010.01.025>
- Dussubieux L, Lankton JW, Bellina-Pryce B, Chaisuwan B (2012) Early Glass Trade in South and Southeast Asia: New Insights from Two Coastal Sites, Phu Khao Thong in Thailand and Arikamedu in South India. In: Tjoa-Bonatz ML, Reinecke A, Bonatz D (eds) *Crossing Borders: Selected Papers from the 13th International Conference of the European Association of Southeast Asian Archaeologists*. NUS Press, pp 307–328.
- Dussubieux L, Pryce TO (2016) Myanmar's role in Iron Age interaction networks linking Southeast Asia and India: Recent glass and copper-base metal exchange research from the Mission Archéologique Française au Myanmar. *J. Archaeol. Sci. Rep.* 5:598–614. <https://doi.org/10.1016/j.jasrep.2016.01.005>
- Eugster HP, Hardie LA (1978) Saline lakes. In: Lerman A (ed) *Lakes: Chemistry, Geology, Physics*. Springer-Verlag, Berlin, pp 237–293.
- Francis P (1988) Glass beads in Asia: part I. Introduction. *Asian Perspectives* 28(1):1–21.
- Francis P (2002) *Asia's maritime bead trade: 300 BC to the present*. University of Hawaii Press.
- Finch AA, Allison N (2007) Coordination of Sr and Mg in calcite and aragonite. *Mineral. Mag.* 71(5):539–552. <https://doi.org/10.1180/minmag.2007.071.5.539>
- Fuxi G (2009) Origin and evolution of ancient Chinese glass. In: Fuxi G, Brill RH, Shouyun T (eds) *Ancient glass research along the Silk Road*. World Scientific, pp 1–40.
- Gu Z, Luo W, Jiang X, Liu N, Fu Y, Zhang L, Yang M, Yang Y (2020) Copper-Red Glass Beads of the Han Dynasty Excavated in Yunnan Province, Southwestern China. *J. Glass Studies* 62:11–22.
- Hall ME, Yablonsky L (1998) Chemical analyses of Sarmatian glass beads from Pokrovka, Russia. *J. Archaeol. Sci.* 25(12):1239–1245. <https://doi.org/10.1006/jasc.1998.0294>
- Hartigan JA (1975) *Clustering algorithms*. John Wiley & Sons, Inc, Hoboken.
- Henderson J (2013) *Ancient glass: an interdisciplinary exploration*. Cambridge University Press.

- Jackson CM, Booth CA, Smedley JW (2005) Glass by design? Raw materials, recipes and compositional data. *Archaeometry* 47(4):781–795. <https://doi.org/10.1111/j.1475-4754.2005.00232.x>
- Jackson CM, Nicholson PT (2010) The provenance of some glass ingots from the Uluburun shipwreck. *J. Archaeol. Sci.* 37(2):295–301. <https://doi.org/10.1016/j.jas.2009.09.040>
- Jackson CM, Paynter S, Nenna MD, Degryse P (2018) Glassmaking using natron from el-Barnugi (Egypt); Pliny and the Roman glass industry. *Archaeol. Anthropol. Sci.* 10:1179–1191. <https://doi.org/10.1007/s12520-016-0447-4>
- Jochum KP, Weis U, Stoll B, Kuzmin D, Yang Q, Raczek I, Jacob DE, Stracke A, Birbaum K, Frick D, Günther D, Enzweiler J (2011) Determination of reference values for NIST SRM 610–617 glasses following ISO guidelines. *Geostand. Geoanal. Res.* 35(4):397–429. <https://doi.org/10.1111/j.1751-908X.2011.00120.x>
- Kemp V, Brownscombe W, Shortland A (2022) The investigation and provenance of glass vessel fragments attributed to the Tomb of Amenhotep II, KV35, Valley of the Kings. *Archaeometry* 64(1):147–160. <https://doi.org/10.1111/arcn.12687>
- Lankton JW, Dussubieux L (2013) Early glass in southeast Asia. In: Janssens K (ed) *Modern methods for analysing archaeological and historical glass*, 1, John Wiley & Sons, pp 415–443.
- Lankton JW, Dussubieux L, Gratuze B (2006) Glass from Khao Sam Kaeo: transferred technology for an early Southeast Asian exchange network. *Bulletin de l'École française d'Extrême-Orient* 93:317–351.
- Laugié M, Michel J, Pohl A, Poli E, Borgomano J (2019) Global distribution of modern shallow-water marine carbonate factories: a spatial model based on environmental parameters. *Sci. Rep.* 9(1):16432. <https://doi.org/10.1038/s41598-019-52821-2>
- Lee BK (2023) The structure of Mahan society in Baekpo Bay of Haenam Peninsula through external exchange. *J. Mahan-Baekje Cult. Res. Inst.* 41:60–85. <https://doi.org/10.34265/mbmh.2023.41.60>
- Lee BK, Song JS, Lee SK (2022) Excavation report of a mounded twin tombs in Naedong-ri, Yeongam, Jeollanam-do Province, rep. 14. Jeonnam Research Institute of Cultural Heritage, pp 1–95.
- Li QH, Liu S, Zhao HX, Gan FX, Zhang P (2014) Characterization of some ancient glass beads unearthed from the Kizil reservoir and Wanquan cemeteries in Xinjiang, China. *Archaeometry* 56(4):601–624. <https://doi.org/10.1111/arcn.12031>
- Li YHM, Zhao WW, Zhou MF (2017) Nature of parent rocks, mineralization styles and ore genesis of

- regolith-hosted REE deposits in South China: An integrated genetic model. *J. Asian Earth Sci.* 148:65–95. <https://doi.org/10.1016/j.jseaes.2017.08.004>
- Lin Y, Liu T, Toumazou MK, Counts DB, Kakoulli I (2019) Chemical analyses and production technology of archaeological glass from Athienou-Malloura, Cyprus. *J. Archaeol. Sci. Rep.* 23:700–713. <https://doi.org/10.1016/j.jasrep.2018.08.011>
- Liu S, Li Q, Gan F (2015) Chemical analyses of potash–lime silicate glass artifacts from the Warring States period in China. *Spectrosc. Lett.* 48(4):302–309. <https://doi.org/10.1080/00387010.2014.886595>
- Liu S, Li QH, Fu Q, Gan FX, Xiong ZM (2013) Application of a portable XRF spectrometer for classification of potash glass beads unearthed from tombs of Han Dynasty in Guangxi, China. *X-Ray Spectrom.* 42(6):470–479. <https://doi.org/10.1002/xrs.2505>
- Liu S, Li QH, Gan F, Zhang P, Lankton JW (2012) Silk Road glass in Xinjiang, China: chemical compositional analysis and interpretation using a high-resolution portable XRF spectrometer. *J. Archaeol. Sci.* 39(7):2128–2142. <https://doi.org/10.1016/j.jas.2012.02.035>
- Longerich HP, Jackson SE, Günther D (1996) Laser ablation inductively coupled plasma mass spectrometric transient signal data acquisition and analyte concentration calculation. *J. Anal. At. Spectrom.* 11:899–904.
- Lü QQ, Henderson J, Wang Y, Wang B (2021) Natron glass beads reveal proto-Silk Road between the Mediterranean and China in the 1st millennium BCE. *Sci. Rep.* 11(1):3537. <https://doi.org/10.1038/s41598-021-82245-w>
- Ma Q, Pollard AM, Yu Y, Li Z, Liao L, Wang L, Li M, Cai L, Ping L, Wen R (2022a) Laser ablation inductively coupled plasma mass spectrometry analysis of potash and m-Na-Al glasses in China—using Kernel methods for trace element analysis. *Herit. Sci.* 10(1):29. <https://doi.org/10.1186/s40494-022-00651-3>
- Ma Q, Wen R, Yu Y, Wang L, Li M, Cai L, Ping L, Zhao Z, Wang D, Wang X, Shi R, Pollard AM (2022b) Laser ablation inductively coupled plasma mass spectrometry analysis of Chinese lead-barium glass: Combining multivariate kernel density estimation and maximum mean discrepancy to reinterpret the raw glass used for producing lead-barium glass. *Archaeol. Anthropol. Sci.* 14(1):9. <https://doi.org/10.1007/s12520-021-01463-5>

- Medeghini L, Botticelli M, Cadena-Irizar AC, Lepri B, Ferrandes AF, Costa M, Barrulas P (2022) Blue shadows of Roman glass artefacts. *Microchem. J.* 179:107526.  
<https://doi.org/10.1016/j.microc.2022.107526>
- Michel J, Lanteaume C, Lettéron A, Kenter J, Morsilli M, Borgomano J (2020) Oligocene and Miocene global spatial trends of shallow-marine carbonate architecture. *J. Geol.* 128(6):563–570.  
<https://doi.org/10.1086/712186>
- Michel J, Laugié M, Pohl A, Lanteaume C, Masse JP, Donnadieu Y, Borgomano J (2019) Marine carbonate factories: a global model of carbonate platform distribution. *Int. J. Earth Sci.* 108:1773–1792. <https://doi.org/10.1007/s00531-019-01742-6>
- Mirti P, Pace M, Malandrino M, Ponzi MN (2009) Sasanian glass from Veh Ardašīr: new evidences by ICP-MS analysis. *J. Archaeol. Sci.* 36(4):1061–1069. <https://doi.org/10.1016/j.jas.2008.12.008>
- Mirti P, Pace M, Negro Ponzi MM, Aceto M (2008) ICP-MS Analysis of Glass Fragments of Parthian and Sasanian Epoch from Seleucia and Veh Ardašīr (Central Iraq). *Archaeometry* 50(3):429–450.  
<https://doi.org/10.1111/j.1475-4754.2007.00344.x>
- Natalicchio M, Pierre FD, Lugli S, Lowenstein TK, Feiner SJ, Ferrando S, Manzi V, Roveri M, Clari P (2014) Did Late Miocene (Messinian) gypsum precipitate from evaporated marine brines? Insights from the Piedmont Basin (Italy). *Geology* 42(3):179–182. <https://doi.org/10.1130/G34986.1>
- Oikonomou A (2018) Hellenistic core formed glass from Epirus, Greece. A technological and provenance study. *J. Archaeol. Sci. Rep.* 22:513–523. <https://doi.org/10.1016/j.jasrep.2018.04.030>
- Oikonomou A, Henderson J, Gnade M, Chenery S, Zacharias N (2018) An archaeometric study of Hellenistic glass vessels: evidence for multiple sources. *Archaeol. Anthropol. Sci.* 10:97–110.  
<https://doi.org/10.1007/s12520-016-0336-x>
- Oikonomou A, Triantafyllidis P (2018) An archaeometric study of Archaic glass from Rhodes, Greece: Technological and provenance issues. *J. Archaeol. Sci. Rep.* 22:493–505.  
<https://doi.org/10.1016/j.jasrep.2018.08.004>
- Olmeda G, Angelini I, Molin G, Boaro S, Leonardi G (2015) Archaeometric analysis of vitreous material ornaments from the Villa di Villa site (Treviso, Italy). *Rend. Lincei* 26:513–527.  
<https://doi.org/10.1007/s12210-015-0452-z>
- Panighello S, Orsega EF, van Elteren JT, Šelih VS (2012) Analysis of polychrome Iron Age glass vessels



- from Mediterranean I, II and III groups by LA-ICP-MS. *J. Archaeol. Sci.* 39(9):2945–2955.  
<https://doi.org/10.1016/j.jas.2012.04.043>
- Peel MC, Finlayson BL, McMahon TA (2007) Updated world map of the Köppen-Geiger climate classification. *Hydrol. Earth Syst. Sci.* 11(5):1633–1644. <https://doi.org/10.5194/hess-11-1633-2007>
- Philpotts AR, Ague JJ (2022) *Principles of igneous and metamorphic petrology*, 3rd edn. Cambridge University Press. <https://doi.org/10.1017/9781108631419>
- Pion C, Gratuze B (2016) Indo-Pacific glass beads from the Indian subcontinent in Early Merovingian graves (5th–6th century AD). *Archaeol. Res. Asia* 6:51–64. <https://doi.org/10.1016/j.ara.2016.02.005>
- Purowski T, Kępa L, Wagner B (2018) Glass on the Amber Road: the chemical composition of glass beads from the Bronze Age in Poland. *Archaeol. Anthropol. Sci.* 10:1283–1302.  
<https://doi.org/10.1007/s12520-016-0443-8>
- R Core Team (2021) *R: A language and environment for statistical computing*. R Foundation for Statistical Computing, Vienna, Austria. <https://www.R-project.org/>
- Rehren T, Freestone IC (2015) Ancient glass: from kaleidoscope to crystal ball. *J. Archaeol. Sci.* 56:233–241. <https://doi.org/10.1016/j.jas.2015.02.021>
- Rösch C, Hock R, Schüssler U, Yule P, Hannibal A (1997) Electron microprobe analysis and X-ray diffraction methods in archaeometry: investigations on pre-Islamic beads from the sultanate of Oman. *Eur. J. Mineral.* 9:763–783. <https://doi.org/10.11588/propylaeumdok.00000305>
- Rudnick RL, Gao S (2014) Composition of the continental crust. In: Holland HD, Turekian KK (eds) *Treatise on Geochemistry*, 2nd ed. Elsevier, Oxford, pp 1–15.
- Saccani E (2015) A new method of discriminating different types of post-Archean ophiolitic basalts and their tectonic significance using Th-Nb and Ce-Dy-Yb systematics. *Geosci. Front.* 6(4):481–501.  
<https://doi.org/10.1016/j.gsf.2014.03.006>
- Saemundsson K (2010) *East African Rift System—An Overview*, presented at Short Course V on Exploration for Geothermal Resources. UNU-GTP, GDC and KenGen. ISBN 978-9979-68-240-0.
- Sayre EV, Smith RW (1961) Compositional categories of ancient glass. *Science*, 133(3467):1824–1826.  
<https://doi.org/10.1126/science.133.3467.18>
- Schibille N, Sterrett-Krause A, Freestone IC (2017) Glass groups, glass supply and recycling in late Roman Carthage. *Archaeol. Anthropol. Sci.* 9:1223–1241. <https://doi.org/10.1007/s12520-016-0316->

- Shortland AJ, Kirk S, Eremin K, Degryse P, Walton M (2018) The analysis of Late Bronze Age glass from Nuzi and the question of the origin of glass-making. *Archaeometry* 60(4):764–783.  
<https://doi.org/10.1111/arcm.12332>
- Silvestri A (2008) The coloured glass of Iulia Felix. *J. Archaeol. Sci.* 35(6):1489–1501.  
<https://doi.org/10.1016/j.jas.2007.10.014>
- Silvestri A, Molin G, Salviulo G (2005) Roman and medieval glass from the Italian area: bulk characterization and relationships with production technologies. *Archaeometry* 47(4):797–816.  
<https://doi.org/10.1111/j.1475-4754.2005.00233.x>
- Stern WB (2017) Phosphate: a neglected argument in studies of ancient glass technology. *Swiss J. Geosci.* 110(3):725–740. <https://doi.org/10.1007/s00015-016-0242-3>
- Tamura T, Oga K (2016) Archaeometrical investigation of natron glass excavated in Japan. *Microchem. J.* 126:7–17. <https://doi.org/10.1016/j.microc.2015.11.029>
- Then-Obłuska J, Dussubieux L (2016) Glass bead trade in the Early Roman and Mamluk Quseir ports—A view from the Oriental Institute Museum assemblage. *Archaeol. Res. Asia* 6:81–103.  
<https://doi.org/10.1016/j.ara.2016.02.008>
- Then-Obłuska J, Dussubieux L (2021) Beads for the nomads of late antiquity: Chemical characterization of glass from the Blemmyan tumuli at Kalabsha, Nubia, of the mid-fourth century CE. *Archaeometry* 63(6):1255–1271. <https://doi.org/10.1111/arcm.12680>
- Then-Obłuska J, Wagner B (2019) Glass beads and pendants from Meroitic and Nobadian lower Nubia, Sudan: Chemical compositional analysis using laser ablation-inductively coupled plasma-mass spectrometry. *Archaeometry* 61(4):856–873. <https://doi.org/10.1111/arcm.12465>
- Torsvik TH, Van der Voo R, Preeden U, Mac Niocail C, Steinberger B, Doubrovine PV, Van Hinsbergen DJ, Domeier M, Gaina C, Tohver E, Meert JG (2012) Phanerozoic polar wander, palaeogeography and dynamics. *Earth Sci. Rev.* 114(3-4):325–368. <https://doi.org/10.1016/j.earscirev.2012.06.007>
- Tosca NJ, Tutolo BM (2023) How to make an alkaline lake: Fifty years of chemical divides. *Elements* 19(1):15–21. <https://doi.org/10.2138/gselements.19.1.15>
- Towle A, Henderson J (2004) The glass bead game: archaeometric evidence for the existence of an Etruscan glass industry. *Etruscan Studies* 10(1):47–66. <https://doi.org/10.1515/etst.2004.10.1.47>

- Tzankova N, Mihaylov P (2019) Chemical characterization of glass beads from the necropolis of Dren-Delyan (6th–4th century BC), Southwest Bulgaria. *Geol. Balc*, 48:31–50.
- Van Ham-Meert A, Dillis S, Blomme A, Cahill N, Claeys P, Elsen J, Eremin K, Gerdes A, Steuwe C, Roeffaers M, Shortland A, Degryse P (2019) A unique recipe for glass beads at Iron Age Sardis. *J. Archaeol. Sci.* 108:104974. <https://doi.org/10.1016/j.jas.2019.104974>
- van Hinsbergen DJ, De Groot LV, van Schaik SJ, Spakman W, Bijl PK, Sluijs A, Langereis CG, Brinkhuis H (2015) A paleolatitude calculator for paleoclimate studies. *PLoS ONE* 10(6):e0126946. <https://doi.org/10.1371/journal.pone.0126946>
- Van Strydonck M, Gratuze B, Rolland J, De Mulder G (2018) An archaeometric study of some pre-Roman glass beads from Son Mas (Mallorca, Spain). *J. Archaeol. Sci. Rep.* 17:491–499. <https://doi.org/10.1016/j.jasrep.2017.12.003>
- Varberg J, Gratuze B, Kaul F (2015) Between Egypt, Mesopotamia and Scandinavia: late bronze age glass beads found in Denmark. *J. Archaeol. Sci.* 54:168–181. <https://doi.org/10.1016/j.jas.2014.11.036>
- Varberg J, Gratuze B, Kaul F, Hansen AH, Rotea M, Wittenberger M (2016) Mesopotamian glass from late bronze age Egypt, Romania, Germany, and Denmark. *J. Archaeol. Sci.* 74:184–194. <https://doi.org/10.1016/j.jas.2016.04.010>
- Vicenzi EP, Eggins S, Logan A, Wysoczanski R (2002) Microbeam Characterization of Corning Archeological Reference Glasses: New Additions to the Smithsonian Microbeam Standard Collection. *J. Res. Nat. Inst. Stand. Tech.* 107(6):719–727. <https://doi.org/10.6028/jres.107.058>
- Wadia DN (1975) *Geology of India*, 4th edn. Tata Mac Graw Hill Publishing Co, New Delhi.
- Walton M, Eremin K, Shortland A, Degryse P, Kirk S (2012) Analysis of Late Bronze Age glass axes from Nippur—A new cobalt colourant. *Archaeometry* 54(5):835–852. <https://doi.org/10.1111/j.1475-4754.2012.00664.x>
- Walton MS, Shortland A, Kirk S, Degryse P (2009) Evidence for the trade of Mesopotamian and Egyptian glass to Mycenaean Greece. *J. Archaeol. Sci.* 36(7):1496–1503. <https://doi.org/10.1016/j.jas.2009.02.012>
- Wang KW, Iizuka Y, Hsieh YK, Lee KH, Chen KT, Wang CF, Jackson C (2019) The anomaly of glass beads and glass beadmaking waste at Jiuxianglan, Taiwan. *Archaeol. Anthropol. Sci.* 11:1391–1405.

<https://doi.org/10.1007/s12520-017-0593-3>

Wang KW, Iizuka Y, Jackson C (2022) The production technology of mineral soda alumina glass: A perspective from microstructural analysis of glass beads in Iron Age Taiwan. *PLoS ONE*

17(2):e0263986. <https://doi.org/10.1371/journal.pone.0263986>

Wang KW, Jackson C (2014) A review of glass compositions around the South China Sea region (the late 1st millennium BC to the 1st millennium AD): placing Iron Age glass beads from Taiwan in context.

*J. Indo-Pac. Archaeol.* 34:51–60. <https://doi.org/10.7152/jipa.v34i0.14701>

Xie YL, Hou Z, Goldfarb RJ, Guo X, Wang L (2016) Rare earth element deposits in China. In: Verplanck PL, Hitzman MW (eds) *Rare Earth and Critical Elements in Ore Deposits, Reviews in Economic*

*Geology*, vol. 18. *Soc. Econ. Geol.* 18:115–136.

## Table captions

Table 1 Median concentration (in wt.%) of seven major elements, categorized by glass type and color, along with the interquartile range (in gray color).

Table S1 (ESM 2) List of literature sources for the geochemical data used in this study.

Table S2 (ESM 2) List of color names and corresponding 6-digit hexadecimal color codes for each color group.

Table S3 (ESM 2) Reference and measured values of major and minor chemical compositions for Corning A, B, and C glasses determined by EPMA.

Table S4 (ESM 2) Chemical composition of glass beads unearthed from a twin tomb at Yeongam, South Korea.

Table S5 (ESM 2) LA-ICP-MS elemental data for the NIST SRM612 standard compared with its reference values.

Table S6 (ESM 2) Trace element concentrations of glass beads unearthed from a twin tomb at Yeongam, South Korea.

## Figure captions

- Fig. 1 Bivariate plots of principal component (PC) scores and loadings for ancient glass data by color. Clusters of ancient glass, categorized by color through *k*-means cluster analysis, are represented on the PC score plane.
- Fig. 2 Spatiotemporal distribution and frequency of occurrence for ancient glass by classified type. The vertical axis of time series data corresponds to square root scale. EU = Europe, AS = Asia, ME = Middle East, and AF = Africa.
- Fig. 3 Sequential variational patterns of minor and trace elements by classified type. Glass data are normalized to the composition of upper crust (Rudnick and Gao 2014). Solid line denotes the median, while the shaded area represents the interquartile range. Open circles in the background correspond to individual data.
- Fig. 4 Upper crust-normalized rare-earth element patterns for different glass types. Normalizing values from Rudnick and Gao (2014). Solid line denotes the median, while the shaded area represents the interquartile range.